Lennard-Jones Parameters Determined to Reproduce the Solubility of NaCl and KCl in SPC/E, TIP3P, and TIP4P/2005 Water

Takuma Yagasaki,[*, †, ‡] Masakazu Matsumoto,[†,‡] and Hideki Tanaka[†,‡]

[†]Research Institute for Interdisciplinary Science, Okayama University, Okayama, 700-8530, Japan

[‡]Department of Chemistry, Faculty of Science, Okayama University, Okayama, 700-8530, Japan

ABSTRACT

Most classical non-polarizable ion potential models underestimate the solubility values of NaCl and KCl in water significantly. We determine Lennard-Jones (LJ) parameters of Na^+, K^+, and Cl^- that reproduce the solubility as well as the hydration free energy in dilute aqueous solutions for three water potential models, SPC/E, TIP3P, and TIP4P/2005. The ion-oxygen distance in the solution and the cation-anion distance in salt are also considered in the parametrization. In addition to the target properties, the hydration enthalpy, hydration entropy, self-diffusion coefficient, coordination number, lattice energy, enthalpy of solution, density, viscosity, and number of contact ion pairs are calculated for comparison with 17 frequently used or recently developed ion potential models. The overall performance of each ion model is represented by a global score using a scheme that was originally developed for comparison of water potential models. The global score is better for our models than for the other 17 models not only because of the quite good prediction for the solubility but also because of the relatively small deviation from the experimental value for many of the other properties.

1. INTRODUCTION

Ion hydration is relevant to various processes such as chemical reactions, biomolecular functions, and atmospheric phenomena.[1-14] Molecular dynamics (MD) simulations have provided a wealth of information on thermodynamic, structural, and dynamic properties of ion hydration. In many cases, the ion-water interaction is described by the classical 12-6-1 type potential function:

$$U(r_{ij}) = 4\varepsilon_{ij} \left\{ \left(\frac{\sigma_{ij}}{r_{ij}}\right)^{12} - \left(\frac{\sigma_{ij}}{r_{ij}}\right)^{6} \right\} + \frac{q_i q_j}{4\pi\varepsilon_0 r_{ij}}, \quad (1)$$

where ε_{ij} and σ_{ij} are the Lennard-Jones (LJ) energy and size parameters, q_i is the partial charge on the i-th interaction site, ε_0 is the permittivity of vacuum, and r_{ij} is the distance between the i-th and j-th interaction sites. The computational cost of the 12-6-1 type potential is low because of its simple form. Therefore, long and/or large-scale all-atom MD simulations are usually performed using the 12-6-1 potential.[15-20]

Solubility of salts in water is an important basic property in solution chemistry. There are two types of techniques to obtain the solubility using MD simulations. One is the chemical potential route in which the chemical potential of salt in the solid phase and that in the aqueous phase are calculated separately using thermodynamic integration or similar methods.[21-22] The other is the direct coexistence method in which the solubility is determined from MD simulations of an aqueous solution in contact with a slab of crystalline salt.[23] Table 1 summarizes the values of solubility of NaCl and KCl in water calculated using the two methods with 12-6-1 type potential models. The values reported in refs. 24, 25, and 26 are much higher than those of the other studies probably due to the artifact arising from the small system size mentioned by Espinosa et al.[27] When the results of these three studies are ignored, only the SPC/E-RDVH (5.7 mol kg^{-1}) and TIP4P/2005-Madrid (5.7 mol kg^{-1}) reproduce the experimental solubility of NaCl (6.1 mol kg^{-1}),

and there is no model that reproduces the solubility of KCl (4.8 mol kg^{-1}) in the table. Most of the models underestimate the solubility to a large extent, and use of such a potential model can cause serious problems in MD simulations. For example, it was reported that ions aggregate spontaneously in the vicinity of biomolecules even when the salt concentration is much lower than the experimental solubility value.[28-32]

Table 1. Solubility of NaCl and KCl in water calculated in simulation studies. The experimental solubility value is 6.1 mol kg^{-1} for NaCl and 4.8 mol kg^{-1} for KCl.[33]

Salt	Water model	Ion model	Solubility / mol kg^{-1}	
			Chemical potential route	Direct coexistence method
NaCl	SPC/E[34]	JC[35]	3.6,[36] 3.7,[21] 3.7[22]	7.3,[24] 5.9,[25] 6.2,[26] 3.7,[27] 3.6[37]
		HMN1[38]	0.0[36]	
		HMN2[38]	1.8[36]	
		HMN3[38]	1.3[36]	
		RH1[39]	0.0[36]	
		RH2[39]	0.0[36]	
		RH3[39]	0.1[36]	
		Dang[40]	0.2[36]	
		RDVH[41]	5.7[21]	
		KBFF[42]	0.9[21]	
		SD[43]	0.6,[21] 0.6[36]	
		CHARMM[44]		2.6[26]
		DVH[45]	6.9[36]	
	TIP3P[46]	JC		1.5[24]
	TIP4P/2005[47]	Madrid[48]	5.7[48]	5.7[48]
KCl	SPC/E	JC	2.7[21]	5.1[24]
		RDVH	0.1[21]	
		KBFF	0.6[21]	
	TIP3P	JC		1.0[24]

The solubility is determined by the balance between the stability of ion in the solution and that in crystalline salt. Joung and Cheatham determined LJ parameters for monovalent ions using the hydration free energy and the lattice energy of salt as target properties.[35] Agreement with the

experimental solubility is better for the models of Joung and Cheatham than for most other models. However, their models still underestimate the solubility. Recently, Benavides et al. proposed a model of NaCl in TIP4P/2005 water, called the Madrid model.[48] The solubility of this model is very close to the experimental value. This model also reproduces several other properties such as the salt concentration dependence of the density of the solution. A characteristic feature of this model is that the charge on each ion particle is scaled by 0.85. When there are ionic species other than Na^+ and Cl^-, their charges must be scaled consistently to satisfy charge neutrality.[49]

In this paper, we propose 12-6-1 type potential models of Na^+, K^+, and Cl^- in aqueous solutions. A set of ion-water parameters determined for a specific water model is not necessarily good for different water models.[35, 50] We select three water models, SPC/E, TIP3P, and TIP4P/2005, and determine a set of ion LJ parameters for each of the water models. The SPC/E model is a three-site water model.[34] This model is selected because it has been used in MD simulations of aqueous electrolyte solutions as well as pure water very frequently.[5-6, 21-22, 24-27, 36-37, 51-52] The TIP3P model is also a three-site water model.[46] This model has been used in most MD simulations of biomolecules because it is the default water model in the AMBER and CHARMM force field sets.[17, 44] The TIP4P/2005 model is a four-site water model.[47] Unlike the three-site models, this model reproduces not only liquid properties but also properties of ice polymorphs unless the pressure is extremely high.[47, 53-55]

We employ the Lorentz-Berthelot combining rules, $\varepsilon_{IW} = \sqrt{\varepsilon_I \varepsilon_W}$ and $\sigma_{IW} = (\sigma_I + \sigma_W)/2$, where ε_I and σ_I are the LJ parameters of the ion particle and ε_W and σ_W are the LJ parameters of the oxygen atom of water. The charge on the ion particle is not scaled. The solubility of salt, hydration free energy of ion, ion-oxygen distance in the solution phase, and cation-anion distance in crystalline salt are considered as the target properties of the parameterization. In addition to

these target properties, the hydration enthalpy, hydration entropy, coordination number of water around the solute, number of contact ion pairs, self-diffusion coefficients of ion and water, lattice energy of salt, enthalpy of solution, density, and viscosity are evaluated for comparison with the 12-6-1 type ion potential models listed in Table 2, which are selected because they were recently developed or have been frequently used in MD studies.

Table 2. Potential models used in this study. The LJ parameters are listed in Table S1 of the Supporting Information.

Water	Ion	Combining rule	Source
SPC/E[34]	This work	Lorentz-Berthelot	
	JC	Lorentz-Berthelot	Joung and Cheatham[35]
	LSM	Lorentz-Berthelot	Li, Song, and Merz[50]
	HMN1	Lorentz-Berthelot	Horinek et al.[38]
	HMN2	Lorentz-Berthelot	Horinek et al.[38]
	HMN3	Lorentz-Berthelot	Horinek et al.[38]
	RH1	Geometric	Reif and Hünenberger[39]
	RH2	Geometric	Reif and Hünenberger[39]
	RH3	Geometric	Reif and Hünenberger[39]
	Dang	Lorentz-Berthelot	Dang[40]
	RDVH	Lorentz-Berthelot	Reiser et al.[41]
	KBFF	Geometric[a)]	Gee et al.[42]
TIP3P[46]	This work	Lorentz-Berthelot	
	JC	Lorentz-Berthelot	Joung and Cheatham[35]
	LSM	Lorentz-Berthelot	Li, Song, and Merz[50]
	CHARMM	Lorentz-Berthelot	Roux[44]
	AMBER	Lorentz-Berthelot	Case et al.[17]
	OPLS	Geometric	Chandrasekhar et al.[56]
TIP4P/2005[47]	This work	Lorentz-Berthelot	
	Madrid[b)]	Given to each pair	Benavides et al.[48]

[a)]The LJ ε parameter for the ion-cation interaction is scaled by 0.75 for Na^+ and 0.8 for K^+.
[b)]The LJ parameters for K^+ are not given in this model. The charges of Na^+ and Cl^- are scaled by 0.85.

2. Methods

2.1 MD simulations

   MD simulations are performed using the GROMACS 4.6 package with a time step of 2 fs.[15-16] The temperature and pressure are maintained at 298 K and 1 bar using a Nosé-Hoover thermostat[57-58] and a Berendsen barostat.[59-60] The particle mesh Ewald method is used for long-range Coulomb interactions with a real-space cutoff length of 0.9 nm.[61-62] LJ interactions are truncated at 0.9 nm and the standard long-range corrections are included in the potential energy and pressure.

2.2. Solubility

   The solubility of salt in water is calculated using the direct coexistence method.[23] Figure 1 shows the initial configuration of a direct coexistence simulation. The system consists of a slab of salt and an aqueous solution. The dimensions of the simulation box are $4.3 \times 4.1 \times 8.6$ nm^3. This system is large enough to avoid the artifact caused by the small system size reported by Espinosa et al.[27] The number of water molecules is fixed to 1864. The number of ion particles, which is different for different initial concentrations of the aqueous solution, is approximately 1900 for each ion.
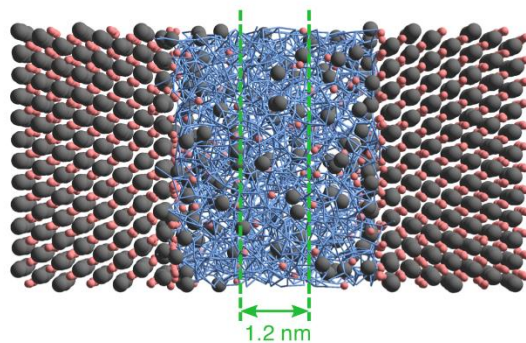

1.2 nm

Figure 1. Initial configuration of a direct coexistence simulation. Red and black spheres show cation and anion particles. The hydrogen bond network of water is represented by blue lines. The concentration of salt in the solution is determined from the numbers of water molecules and ion particles in the region between the dashed green lines.

The concentration of salt in the solution changes as time evolves due to dissolution or growth of the salt slab until the system reaches equilibrium. Both the dissolution and growth rates are minimized when the most stable crystallographic surface, which is {100} for NaCl and KCl, is exposed to the solution.[63] The {111} surface is quite unstable because all particles in a layer have the same charge. This unstable surface is exposed to the solution to facilitate the dissolution and growth of the salt slab in this study. Note that the solubility is independent of the exposed surface.[27]

The concentration at time t, $m(t)$, is calculated from the numbers of salt and water molecules in the bulk region of the solution which is indicated by the green dashed lines in Figure 1. The width of the bulk solution region is 1.2 nm. The number of salt is defined as the average of the numbers of cation particles and that of anion particles.

For each pair of water and ion potential models, three MD simulations are performed for 500 ns at different initial concentrations. When the initial configuration is close to the solubility of the potential model, the concentration of salt in the bulk solution region does not change so much during the simulation. We select one such simulation out of three. As an example, we show the time evolution of the concentration of NaCl calculated using the SPC/E-JC model in Figure 2. It is evident that the initial concentrations of 1 mol kg^{-1} (red) and 6 mol kg^{-1} (blue) are quite different from the solubility value. Therefore, in this case, the simulation started from 3.5 mol kg^{-1} (green) is selected. The selected simulation is continued until the concentration seems to oscillate around

a certain value at least for 500 ns, and the solubility is defined as the concentration averaged over the last 500 ns. Table 3 shows the solubility values obtained from this scheme. Our results are very close to the values obtained via the chemical potential route shown in Table 1.
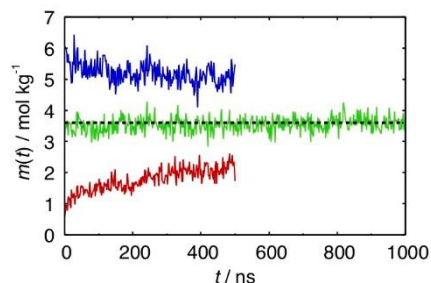

Figure 2. Time evolution of the concentration of NaCl in the bulk solution region for three different initial concentrations, 1 (red), 3.5 (green), and 6 mol kg^{-1} (blue). The SPC/E water model and the JC ion model are employed.

Table 3. Solubility of NaCl and KCl in water at 298 K calculated in this study.

Water model	Ion model	Solubility / mol kg^{-1}	
		NaCl	KCl
SPC/E	This work	6.2 ± 0.29	4.7 ± 0.31
	JC	3.6 ± 0.27	2.8 ± 0.27
	LSM	0.2 ± 0.08	0.1 ± 0.05
	HMN1	0.0 ± 0.04	0.0 ± 0.01
	HMN2	1.5 ± 0.20	0.6 ± 0.13
	HMN3	0.9 ± 0.15	0.3 ± 0.08
	RH1	0.1 ± 0.05	0.4 ± 0.11
	RH2	0.0 ± 0.04	4.7 ± 0.33
	RH3	0.2 ± 0.08	13.3 ± 0.49
	Dang	0.3 ± 0.10	0.3 ± 0.10
	RDVH	5.9 ± 0.29	0.5 ± 0.10
	KBFF	0.9 ± 0.17	0.5 ± 0.13
TIP3P	This work	6.1 ± 0.30	4.7 ± 0.33
	JC	0.2 ± 0.08	0.4 ± 0.11
	LSM	0.1 ± 0.05	0.1 ± 0.06
	CHARMM	0.1 ± 0.05	0.1 ± 0.07
	AMBER	0.0 ± 0.02	0.0 ± 0.02
	OPLS	0.2 ± 0.09	0.1 ± 0.05
TIP4P/2005	This work	6.2 ± 0.28	4.7 ± 0.30
	Madrid	6.0 ± 0.38	
Experiment		6.1	4.8

2.3. Properties of aqueous solutions

The hydration free energy of ion in the limit of a dilute aqueous solution, G_{hyd}, can be divided into two parts,

$$G_{hyd} = G_{LJ} + G_c, \qquad (2)$$

where G_{LJ} is the hydration free energy of the solute without partial charge and G_c is the free energy change for charging the neutral solute. We use the soft-core potential technique to avoid numerical instability in the calculation of G_{LJ}.[64] The potential energy of the system is expressed as

$$U(\lambda_{LJ}) = U_{WW} + \lambda_{LJ} \sum_{j=1}^{N_W} 4\varepsilon_{IW} \left\{ \left(\frac{\sigma_{IW}}{r'_{Ij}(\lambda_{LJ})} \right)^{12} - \left(\frac{\sigma_{IW}}{r'_{Ij}(\lambda_{LJ})} \right)^{6} \right\}, \qquad (3)$$

where U_{ww} is the total water-water interaction energy, N_w is the number of water molecules, and $r'_{Ij}(\lambda_{LJ})$ is the λ-dependent distance between the solute ion and the j-th water molecule. The λ-dependent distance is given by

$$r'_{Ij}(\lambda_{LJ}) = \left\{\alpha\sigma_{Ij}^{48}(1 - \lambda_{LJ}) + r_{Ij}^{48}\right\}^{1/48}, \quad (4)$$

where α is the soft-core parameter which is set to 0.002. The LJ part of the free energy is calculated from

$$G_{LJ} = \sum_{i=0}^{N_\lambda}\left(G\left(\lambda_{LJ}^{(i+1)}\right) - G\left(\lambda_{LJ}^{(i)}\right)\right), \quad (5)$$

with

$$\lambda_{LJ}^{(i)} = \frac{i}{N_\lambda + 1}, \quad (6)$$

where N_λ is the number of intermediate states, which we set $N_\lambda = 19$ in this study. The free energy difference between adjacent states, $G\left(\lambda_{LJ}^{(i+1)}\right) - G\left(\lambda_{LJ}^{(i)}\right)$, is calculated using the acceptance ratio method:

$$G\left(\lambda_{LJ}^{(i+1)}\right) - G\left(\lambda_{LJ}^{(i)}\right) = \frac{C}{\beta}, \quad (7)$$

with

$$\langle(1 + \exp(\beta U_{i+1} - \beta U_i - C))^{-1}\rangle_i = \langle(1 + \exp(\beta U_i - \beta U_{i+1} + C))^{-1}\rangle_{i+1}, \quad (8)$$

where β is the reciprocal temperature and $\langle\ \rangle_i$ represents the ensemble average obtained with the potential energy $U(\lambda_{LJ}^{(i)})$.[65] We perform an equilibration run of 0.1 ns followed by a production run of 1 ns for each $\lambda_{LJ}^{(i)}$.

The free energy change for charging the solute particle, G_c, is calculated in a similar way but with a different λ-dependent potential:

$$U(\lambda_c) = U_{WW} + U_{IW}^{LJ} + \lambda_C \sum_{j=1}^{N_W} \sum_{k=1}^{N_s} \frac{q_I q_k^{(j)}}{4\pi\varepsilon_0 r_{Ik}} , \qquad (9)$$

where U_{IW}^{LJ} is the LJ interaction energy between the solute particle and water, N_s is the number of the charge sites in a water molecule, $q_k^{(j)}$ is the partial charge on the k-th charge site in the j-th water molecule, and q_I is the charge on the solute ion which is either e or $-e$ in this study. The number of intermediate states for the charging is also 19.

The free energy calculations are performed with $N_W = 511$. We check the system size effect on G_{hyd} for the SPC/E-JC model. The calculated G_{hyd} for Na$^+$ with $N_W = 511$, 2047, and 8191 are -371, -371, and -370 kJ mol^{-1}, respectively.

We calculate G_{hyd} of Na$^+$ in an aqueous solution consisting of 510 water molecules and one Cl$^-$ ion to examine the effect of the counter ion. The obtained G_{hyd} value of -370 kJ mol^{-1} is almost the same as that calculated without the counter ion, -371 kJ mol^{-1}. The hydration free energy is not affected by net electric neutrality.[35]

The simulation time of 1 ns for each state is long enough. We perform five independent sets of free energy calculations and obtain $G_{hyd} = -371.4$, -371.5, -371.1, -371.2, and -371.4 kJ mol^{-1}. The standard deviation is only 0.14 kJ mol^{-1}.

The enthalpy of the system, the self-diffusion coefficient of ion, and the ion-oxygen radial distribution function (RDF) are also calculated with the 511-water system. The simulation time is 100 ns. Table S2 shows that this simulation time is long enough to calculate those properties. An MD simulation is performed without the solute to calculate the enthalpy of pure water, H_0. The hydration enthalpy, H_{hyd}, is given by

$$H_{hyd} = H_s - H_0, \qquad (10)$$

where H_s is the enthalpy of the system with the solute particle. The hydration entropy is obtained from the hydration enthalpy and free energy:

$$S_{\text{hyd}} = \frac{H_{\text{hyd}} - G_{\text{hyd}}}{T}. \qquad (11)$$

The self-diffusion coefficient depends on the system size. Figure 3 shows the diffusion coefficients of Na^+ and Cl^- at several salt concentrations calculated for two system sizes. The sum of the number of water molecules and the number of ion particles is 512 and 5120 for the small (open squares) and large systems (open triangles), respectively. The diffusion coefficient is larger for the larger system. Yeh and Hummer showed that the size dependence of the diffusion coefficient is expressed by

$$D(L) = D_\infty - \frac{2.837 k_B T}{6\pi\eta L}, \qquad (12)$$

where D_∞ is the diffusion coefficient in an infinite system, L is the dimension of the simulation cell ($L = 2.48$ nm for the small system and 5.35 nm for the large system), and η is the shear viscosity of the solvent.[66] We calculate the viscosity of pure water using the Green-Kubo formula:

$$\eta = \frac{V}{k_B T} \int_0^\infty \langle P_{\alpha\beta}(t) P_{\alpha\beta}(0) \rangle dt, \qquad (13)$$

where V is the volume of the system and $P_{\alpha\beta}$ is the off-diagonal components of the pressure tensor.[67] The filled symbols in Figure 3 show the values of D_∞ estimated from the viscosity and $D(L)$. The diffusion coefficients of the large and small systems become almost the same when the finite-size correction is included. The corrected value can be compared with the experimental value. The model used to plot Figure 3, SPC/E-JC, reproduces the diffusion coefficient of Na^+ well while it underestimates the diffusion coefficient of Cl^-.
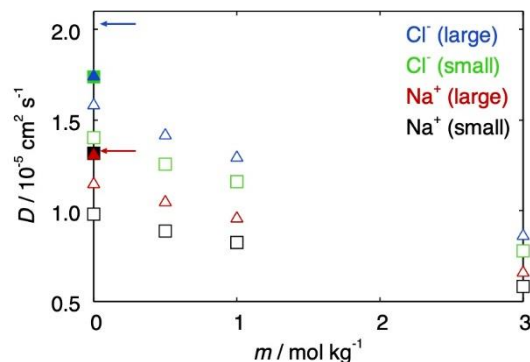
Figure 3. Diffusion coefficients of Na^+ and Cl^- calculated with (filled) and without (open) the finite-size correction of Yeh and Hummer.[66] The SPC/E-JC model is employed. The black and green symbols are those of the small system (the sum of the number of water molecules and the number of ion particles is 512) and the red and blue are those of the large system (the sum is 5120). The value at 0 mol kg^{-1} is calculated with the system consisting of one ion particle and 511 or 5119 water molecules. The red and blue arrows indicate the experimental diffusion coefficients of Na^+ and Cl^- obtained from the ionic conductivities at infinite dilution.[33, 68-69]

2.4. Properties of NaCl and KCl crystals

The lattice constant, potential energy, and enthalpy of salt are calculated with a cubic simulation cell containing 500 cation and 500 anion particles. An equilibration run of 0.1 ns is followed by a production run of 0.3 ns. To check the statistical errors, we perform five independent MD simulations of NaCl with the SPC/E-JC ion model. The cation-anion distance obtained from the lattice constant is 0.2890 nm and the potential energy is -785.5 kJ mol^{-1} for all the five simulations, showing that the simulation time is long enough. We also calculate the lattice energy of salt defined as the potential energy of the salt in which all ion particles are fixed at their equilibrium lattice positions. The density of the salt is set to be the same as that obtained from the MD simulation at 298 K and 1 bar.

14

2.5. Parameterization

The hydration free energy, the ion-oxygen distance defined as the peak position of the RDF of the dilute aqueous solution, the cation-anion distance in salt, and the solubility of salt in water are considered in the parameterization.

First, we calculate the hydration free energy, G_{hyd}, of an ion particle of $\varepsilon_I = 0.0001$ kJ mol^{-1} at several σ_I values. The obtained G_{hyd} values are shown by red squares in Figure 4a. The G_{hyd} value increases with increasing σ_I because of the increase in the cavity formation energy and the weakening of the ion-water coulomb interactions. The horizontal dotted line indicates the experimental G_{hyd} value for Na$^+$ reported by Schmid, Miah, and Sapunov of -371 kJ mol^{-1}.[70] The σ_I value at the intersection of the horizontal line and the cubic spline curve (red solid) is 0.4368 nm. Then, ε_I is multiplied by 2.5 and the σ_I value at the intersection, 0.4092 nm, is determined in the same way (green). This process is repeated until ε_I exceeds 5 kJ mol^{-1}. In Figure 4b, the σ_I value at the intersection is plotted as a function of ε_I. The σ_I value decreases with increasing ε_I. A similar result was reported by Joung and Cheatham.[35] As shown in Figure S1, the effect of an increase in ε_I on the LJ potential is similar to that of an increase in σ_I. Therefore, an increase in ε_I and a simultaneous decrease in σ_I can yield a similar LJ potential that results in the same hydration free energy. The relation between σ_I and ε_I is approximated by the following polynomial function:

$$\sigma_I = \sum_{i=0}^{4} a_i (\log_{10} \varepsilon_I)^i. \quad (14)$$

The coefficients a_i for all the ion species and water models are listed in Table S3. The best fit curve is shown in Figure 4b. The experimental G_{hyd} value is reproduced by a pair of LJ ε_I and σ_I parameters corresponding to any point on this curve.
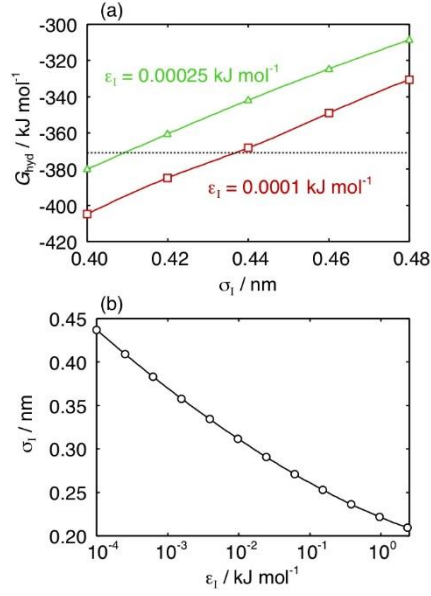
15

Figure 4. (a) Hydration free energies of a cation particle of $\varepsilon_I = 0.0001$ kJ mol^{-1} (red squares) and those of a cation particle of $\varepsilon_I = 0.00025$ kJ mol^{-1} (green triangles) in SPC/E water. The solid curves are obtained from the cubic spline interpolation method. The horizontal dotted line indicates the experimental G_{hyd} value of Na$^+$, -371 kJ mol^{-1}. (b) σ_I value that reproduces the experimental G_{hyd} of Na$^+$ plotted against ε_I. The solid curve is the best fit to Eq. 14.

The solubility of salt in water is determined by the balance between the stability of the ions in water and that in salt. In this study, the LJ parameters of the ions are restricted to satisfy Eq. 14, meaning that the stability in water is fixed and thus the solubility must be tuned by changing the stability in salt. While the SPC/E-JC model reproduces well the experimental G_{hyd}, the solubility of this model (3.6 mol kg^{-1} for NaCl and 2.8 mol kg^{-1} for KCl) is lower than the corresponding experimental value (6.1 mol kg^{-1} for NaCl and 4.8 mol kg^{-1} for KCl) as shown in Table 3. The potential energies of crystalline NaCl and KCl are $E_{salt}^{NaCl} = -785$ kJ mol^{-1} and $E_{salt}^{KCl} = -713$ kJ mol^{-1} for the SPC/E-JC model. We attempt ion LJ parameters that reproduce the experimental G_{hyd} value but yield a potential energy of salt somewhat higher than the SPC/E-JC model because the

solubility of such parameters is expected to be higher than that of the SPC/E-JC model. As a first attempt, we calculate the solubility with $(\sigma_{Na}, \varepsilon_{Na}) = (0.2094 \text{ nm}, 2.375 \text{ kJ mol}^{-1})$, $(\sigma_K, \varepsilon_K) = (0.2756 \text{ nm}, 3.307 \text{ kJ mol}^{-1})$, and $(\sigma_{Cl}, \varepsilon_{Cl}) = (0.4965 \text{ nm}, 0.03433 \text{ kJ mol}^{-1})$. The potential energies of NaCl and KCl for this parameter set are $E_{salt}^{NaCl} = -777.6 \text{ kJ mol}^{-1}$ and $E_{salt}^{KCl} = -705.2 \text{ kJ mol}^{-1}$. We find that it is impossible to reproduce the experimental ion-oxygen distance and the cation-anion distance simultaneously when E_{salt} is close to those values. Therefore, the LJ parameters are determined so that the squared deviation from the experimental value for the ion-oxygen distance becomes almost the same as that for the cation-anion distance. Figure 5a shows the time evolution of the salt concentration in the aqueous solutions for the trial LJ parameter set. The initial concentration is set to be the same as the experimental solubility value in this direct coexistence simulation. As expected, the solubility of this parameter set is higher than that of the SPC/E-JC model, but the value is too high compared with the experimental value, especially for KCl. Therefore, we attempt a different set of LJ parameters that yields somewhat lower potential energies, $E_{salt}^{NaCl} = -781.4 \text{ kJ mol}^{-1}$ and $E_{salt}^{KCl} = -709.1 \text{ kJ mol}^{-1}$. The parameters are $(\sigma_{Na}, \varepsilon_{Na}) = (0.2144 \text{ nm}, 1.596 \text{ kJ mol}^{-1})$, $(\sigma_K, \varepsilon_K) = (0.2784 \text{ nm}, 2.375 \text{ kJ mol}^{-1})$, and $(\sigma_{Cl}, \varepsilon_{Cl}) = (0.5029 \text{ nm}, 0.02742 \text{ kJ mol}^{-1})$. As shown in Figure 5b, this parameter set reproduces the solubility of KCl but underestimates the solubility of NaCl, suggesting that E_{salt}^{NaCl} should be increased leaving E_{salt}^{KCl} almost unchanged. The third trial parameter set is $(\sigma_{Na}, \varepsilon_{Na}) = (0.2117 \text{ nm}, 1.973 \text{ kJ mol}^{-1})$, $(\sigma_K, \varepsilon_K) = (0.2791 \text{ nm}, 2.223 \text{ kJ mol}^{-1})$, and $(\sigma_{Cl}, \varepsilon_{Cl}) = (0.5029 \text{ nm}, 0.02742 \text{ kJ mol}^{-1})$. The potential energies of this set are $E_{salt}^{NaCl} = -778.9 \text{ kJ mol}^{-1}$ and $E_{salt}^{KCl} = -709.9 \text{ kJ mol}^{-1}$. Figure 5c shows that this parameter set reproduces the solubility very well for both salts. The parameter sets for the TIP3P and TIP4P/2005 water models are determined in the same manner. The final parameter sets are listed in Table 4.
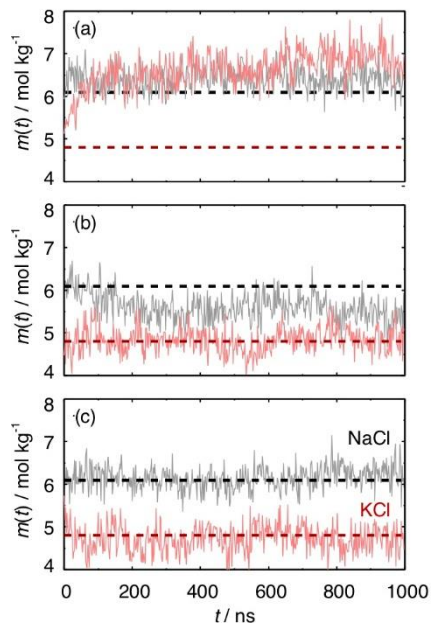
Figure 5. Time evolution of the concentration of NaCl (gray) and KCl (red) for the (a) first, (b) second, and (c) third trial parameter sets for SPC/E water. The horizontal dashed lines indicate the experimental solubility values.

Table 4. Final LJ parameter sets.

		σ_I / nm	ε_I / kJ mol^{-1}
SPC/E	Na$^+$	0.2117	1.973
	K$^+$	0.2791	2.223
	Cl$^-$	0.5029	0.02742
TIP3P	Na$^+$	0.2245	1.275
	K$^+$	0.2906	1.847
	Cl$^-$	0.6522	0.0002458
TIP4P/2005	Na$^+$	0.2032	1.871
	K$^+$	0.2723	1.973
	Cl$^-$	0.5244	0.01750

In standard classical MD simulations, including this study, neither nuclear quantum effects nor multi-body interactions arising from polarization and charge transfer are not explicitly included. These effects are included effectively in the ion LJ parameters to reproduce the experimental

18

properties. In such a case, the LJ energy parameter, ε_I, cannot be considered as a parameter that solely represents the strength of the van der Waals (vdW) interactions. Therefore, ε_I for Cl$^-$ can be smaller than those for the cations as a result of parameterization. As shown in Table S1, this feature is not unique to our parameter sets.

3. RESULTS AND DISCUSSIONS

We compare the ion models listed in Table 2. Experimentally, not the hydration free energy of each ion, G_{hyd}, but that of the cation-anion pair, $G_{pair} = G_{cation} + G_{anion}$, is measured. Experimental G_{hyd} values depend strongly on assumptions made to determine them from a set of G_{pair} values. For example, G_{hyd} of Cl$^-$ determined by Schmid et al. is lower than that of Marcus by 33 kJ mol^{-1}.[70-71] G_{hyd} of an ion potential model can be different from that of another model when the two models are parameterized on the basis of different experimental G_{hyd} values. To avoid this problem, we compare the ion models using G_{pair} as shown in Figure 6 (the calculated G_{hyd} values are listed in Table S4). A large deviation from the experimental value is observed for relatively old ion models such as SPC/E-Dang because they were parameterized without free energy calculations that had been computationally expensive. The G_{pair} value of the TIP4P/2005-Madrid model is much higher than the experimental value because the charge on the ion is scaled by 0.85.
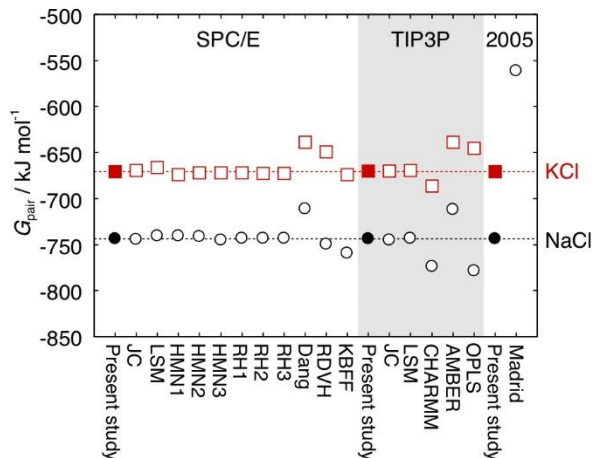
19

Figure 6. Hydration free energies of NaCl (black circles) and KCl (red squares). The horizontal dotted lines indicate the experimental values.[70] The corresponding numerical data are given in S5. It is possible to estimate the Henry's law standard state chemical potential of salt, $\mu^{\dagger}$, from G_{pair} and the dielectric permittivity of water.[72] The calculated $\mu^{\dagger}$ values are listed in table S6 together with the experimental values.[73] The dielectric permittivity of water is taken from ref. 74. The deviation from the experimental $\mu^{\dagger}$ value is small for models that reproduce G_{pair}.

Figure 7a shows the hydration enthalpies of NaCl and KCl. This figure is quite similar to Figure 6. Figure 7b shows the hydration entropies. This property seems to depend rather on the water model than on the ion parameters: the entropies calculated with SPC/E and TIP4P/2005 tend to be higher than those calculated with TIP3P. The negative entropy is mainly because of the water molecules in the first hydration shell that are tightly bound to the ion due to the strong ion-water Coulomb attractions. However, the tight first hydration shell can be disturbed by water molecules in outer hydration shells. This disturbance, which results in increase in the entropy, would be significant when the water-water attractive interactions are strong. The vaporization enthalpy, which reflects the strength of the water-water attraction, is 50.2, 49.3, and 42.1 kJ mol^{-1} for

TIP4P/2005, SPC/E, and TIP3P, respectively.[74] Therefore, the hydration entropy is higher for TIP4P/2005 and SPC/E than for TIP3P.
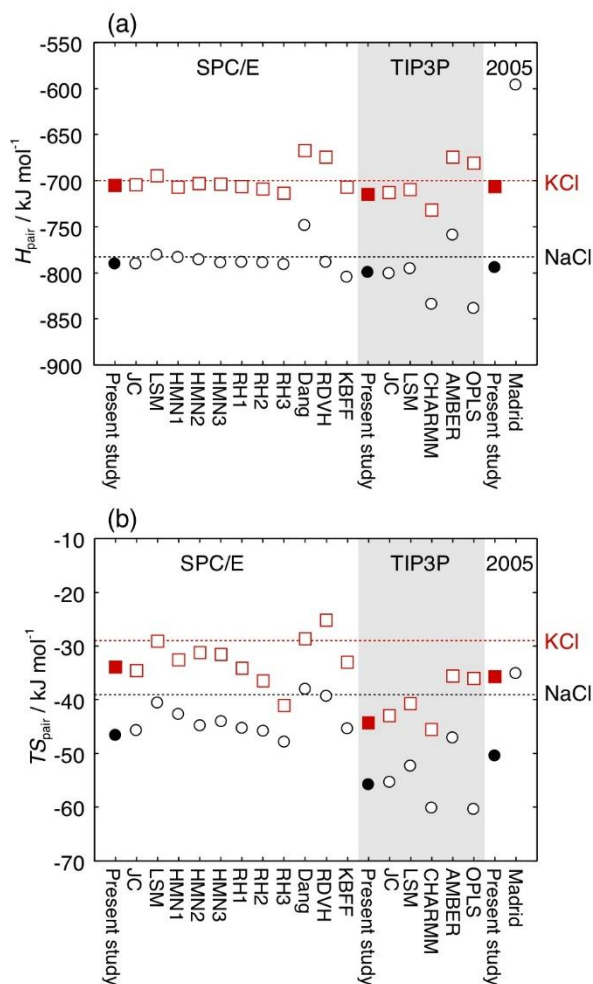

Figure 7. (a) Hydration enthalpy and (b) entropy for NaCl (black circles) and KCl (red squares). The horizontal dotted lines indicate the experimental values.[70] The corresponding numerical data are given in Table S5.

The self-diffusion coefficients of Na^+, K^+, and Cl^- at infinite dilution are shown in Figure 8. This property also depends more on the water model than on the ion model. An ion particle moves in liquid water as a cluster consisting of the solute particle and tightly bound surrounding solvent molecules.[75-76] The interactions between the water molecules in the first hydration shell and those

in outer hydration shells are more important than the ion-water interactions for the diffusion process of this cluster. The diffusion coefficient of ion is very large in TIP3P water because of its weak water-water interactions. The SPC/E model reproduces well the self-diffusion coefficient of water molecules in pure water.[74] The diffusion coefficient of ion in SPC/E water is also close to the experimental value.
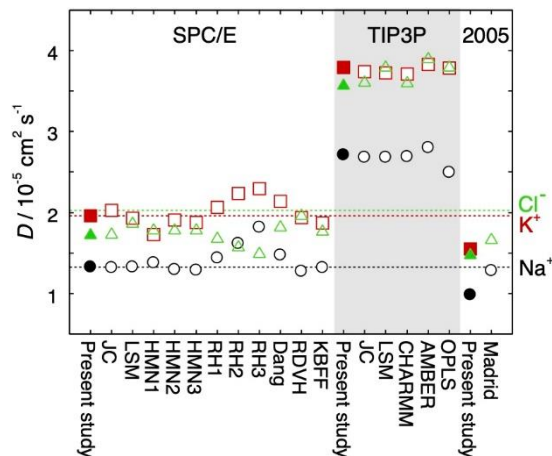

Figure 8. Self-diffusion coefficients of Na^+ (black circles), K^+ (red squares), and Cl^- (green triangles) at infinite dilution including the finite-size correction of Yeh and Hummer.[66] The viscosities of pure water used to estimate the corrections are 0.738, 0.329, and 0.884 mPa s for the SPC/E, TIP3P, and TIP4P/2005 models, respectively. The horizontal dotted lines indicate the experimental values.[33, 68-69] The corresponding numerical data are given in Table S7. The diffusion coefficients at 3 mol kg^{-1} are also shown in the table.

Figure 9a presents the ion-oxygen distance in the solution at infinite dilution. The horizontal dotted lines indicate the average of experimental values reported in a review paper of Ohtaki and Radnai.[3] As mentioned above, it is impossible to reproduce simultaneously the solubility, hydration free energy, ion-oxygen distance, and cation-anion distance. Therefore, we allow for deviations from the experimental values for the ion-oxygen distance and the cation-anion distance

22

to the same extent. The ion-oxygen distance predicted by our model is shorter than the experimental value for all the ion species and the water models. However, the deviation is satisfactorily small.
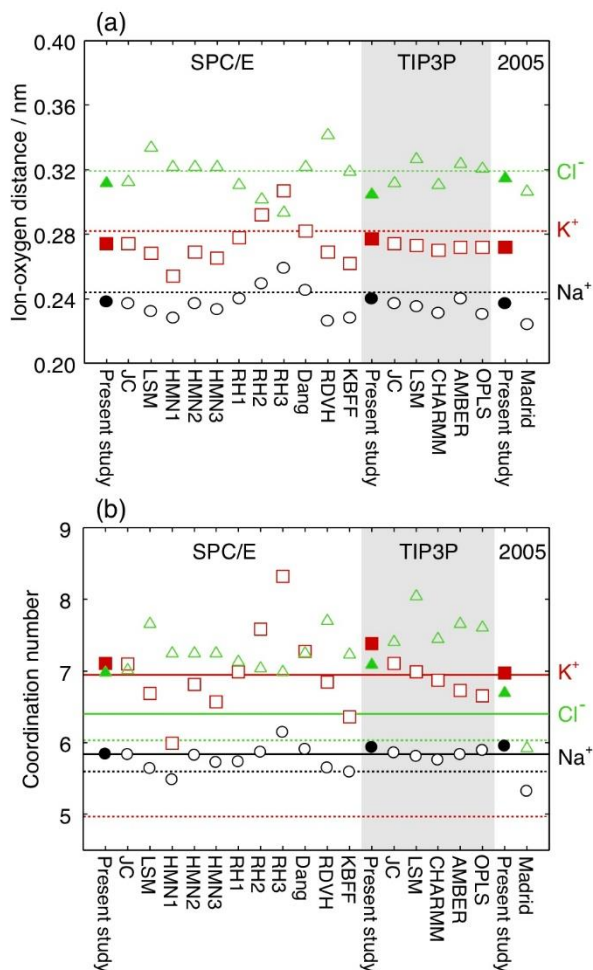

Figure 9. (a) Ion-oxygen distance and (b) coordination number for Na^+ (black circles), K^+ (red squares), and Cl^- (green triangles) in water. The horizontal dotted lines indicate the average of experimental values reported in a review paper of Ohtaki and Radnai.[3] The solid lines in panel (b) are the averages of QM MD simulations.[77-79] The corresponding numerical data are given in Table S8.

The coordination number is defined as the number of solvent molecules in the first solvation shell of the solute. Experimental coordination numbers are not so accurate for monovalent ions due to the low sensitivity at the distance corresponding to the first minimum in the RDF.[1, 3, 80-81] In addition, the coordination number depends on the concentration and combination of ions in aqueous solutions. As a result, reported experimental coordination numbers are widespread. For example, the coordination number for Na^+ listed in the review of Ohtaki and Radnai ranges from 4.0 to 8.0.[3] The coordination number averaged over the experimental values in the review is shown by the dotted line in Figure 9b. The average is smaller for K^+ than for Na^+. This is quite strange. Several very old experimental results are excluded in a review paper of Marcus,[1] and relatively new values are summarized in a different review of the same author.[2] The coordination number of Na^+ averaged over the values in the two reviews of Marcus, 5.6, is smaller than that of K^+, 6.7. However, the range of the reported coordination numbers, which is 4 to 8 for Na^+, is still very wide. Quantum mechanical (QM) MD simulations might be more reliable than experiments as for this property. The coordination number calculated using the second order Møller-Plesset method and the values obtained from density function theory (DFT) based MD simulations with vdW corrections fall in a narrow range of 5.6-6.1 for Na^+ (we do not consider Hartree-Fock or DFT-based MD simulations without vdW corrections because such simulations underestimate the coordination number for small monovalent ions).[77-79] The coordination number averaged over the QM MD studies is shown by the solid line in Figure 9b. It was suggested that the small difference, say ~1, in the coordination numbers between Na^+ and K^+ plays an important role in the selectivity of potassium channels.[82-84] Roughly half of the classical ion models, including our models, reproduce this difference precisely. The coordination numbers of Cl^- calculated from the classical ion models are higher than those from the QM MD studies except for the TIP4P/2005-Madrid

model. Some special treatment such as the scaling of the ion-water Coulomb interactions and inclusion of polarization would be necessary to reproduce this property.

We calculate the viscosity, diffusion coefficient, and density at a finite concentration. We choose $m = 3$ mol kg^{-1} as an intermediate concentration both for NaCl and KCl. The numbers of salt and water molecules are 25 and 462, respectively. The simulation time is 100 ns. The viscosity is presented in Figure 10a. The results of SPC/E-RH2 for NaCl, SPC/E-HMN1 and TIP3P-AMBER for NaCl and KCl are not shown because formation of crystalline salt is observed in the simulation. Each value is divided by the value at $m = 0$ mol kg^{-1} in order to focus on the effect of salt. All the ion models overestimate significantly the increase in the viscosity caused by the increase in salt concentration. Figure 10b shows the ratio of the diffusion coefficient of water at 3 mol kg^{-1} to that of pure water. As expected from the viscosity, the ratio of the diffusion coefficient is much lower than the corresponding experimental value for all the models. An increase in the salt concentration causes too much slowing down of dynamics of the solution in classical MD simulations.[85] This problem can be solved when the charge transfer effect is explicitly included, although the computational cost of such a model is much higher than that of the 12-6-1 type models.[86] The use of scaled charge also improve this problem.[49, 87-88] Indeed, the TIP4P/2005-Madrid model is one of the best models for those properties, though the deviation from the experimental value, ~20%, is still large compared with the error for most of the other properties examined in this study. Figure 10c presents the ratio of the density at 3 mol kg^{-1} to that of pure water. Unlike the dynamic properties, the change in the density is well predicted by the classical 12-6-1 type models. The error is only ~2.5% even for TIP3P-CHARMM.
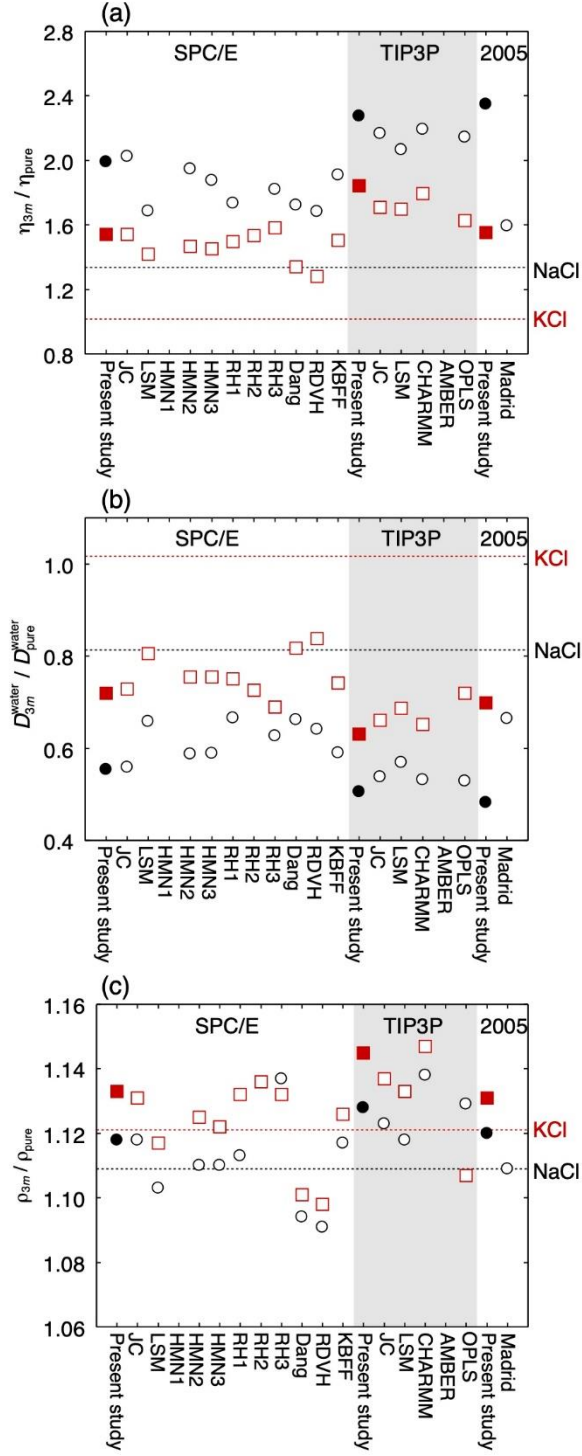
Figure 10. (a) Viscosity, (b) diffusion coefficient of water, and (c) density of the NaCl (black circles) and KCl (red squares) solutions at 3 mol kg^{-1}. Each value is divided by the value at 0

mol kg^{-1}. The horizontal dotted lines indicate the experimental values.[89-91] The corresponding

numerical data and the values at 0 mol kg^{-1} are given in Table S9.

Figure 11a presents the cation-anion distance in salt. Our models overestimate the Na-Cl and

K-Cl distances, but the deviation is small for both salt. The lattice energies of the two crystals are

shown in Figure 11b. The lattice energy of the TIP4P/2005-Madrid model is much higher than the

experimental one again because of the charge scaling. Our models reproduce well the lattice energy

both for NaCl and KCl although this property is not a parametrization target. Figure 11c shows the

enthalpy of solution at infinite dilution calculated from the enthalpy of salt, H_{salt}, and the hydration

enthalpy shown in Figure 7a, H_{pair}:

$$\Delta H_{sol} = H_{pair} - H_{salt}. \quad (15)$$

Dissolution of NaCl in water is endothermic in experiments. However, this process becomes

exothermic for many models including our models. The discrepancy from the experimental value

is also large for KCl. It is difficult to reproduce ΔH_{sol} because this property is determined by the

difference between the two much larger values, H_{pair} and H_{salt}, which are approximately −800 kJ

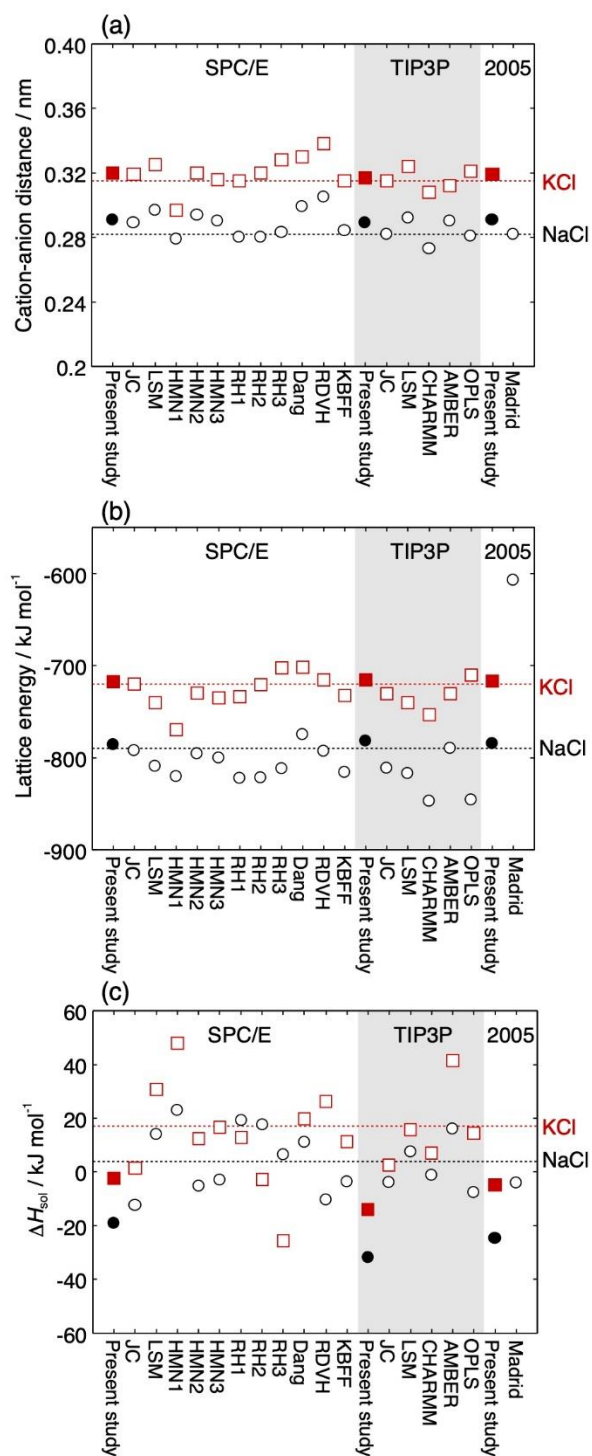mol^{-1} for NaCl and −700 kJ mol^{-1} for KCl.

Figure 11. (a) Cation-anion distance in salt, (b) lattice energy, and (c) enthalpy of solution at infinite dilution for NaCl (black) and KCl (red). The horizontal dotted lines indicate the

28

experimental values.[33, 92] The corresponding numerical data are given in Table S10. The enthalpy of solution at 0.5, 1.0, and 3 mol kg^{-1} are shown in Figure S2 for several models.

Figure 12a shows the solubility of salt. Most of the ion models underestimate this property significantly. Our models and the TIP4P/2005-Madrid model reproduce well the solubility by design. The deviation from experiment is not so large for the SPC/E-JC model because the lattice energy was taken into account in the parameterization. The SPC/E-RDVH model and the SPC/E-RH2 model reproduce the solubility of NaCl and that of KCl, respectively, although they are parameterized without considering this property.
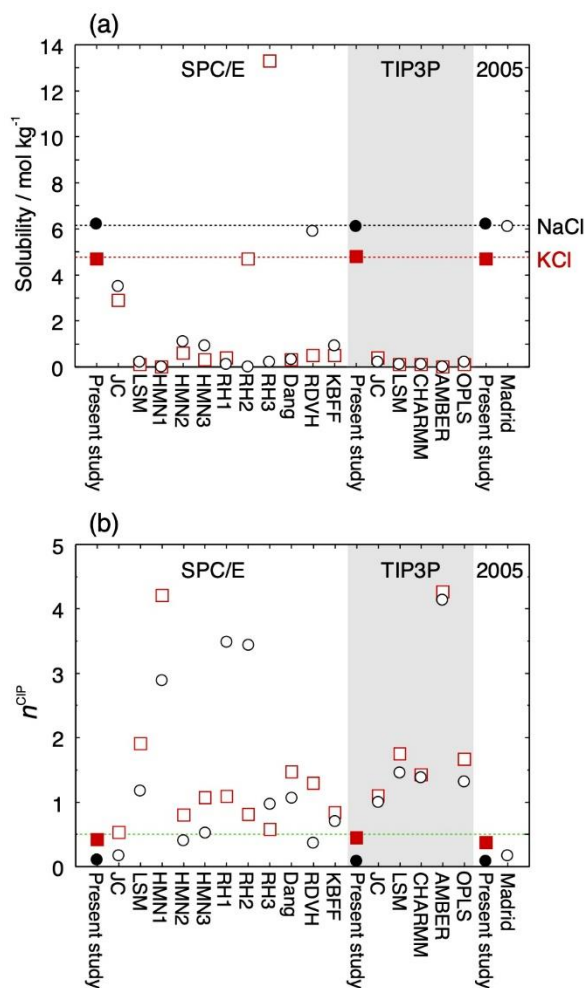

29

Figure 12. (a) Solubility of NaCl (black circles) and KCl (red squares) in water. The horizontal dotted lines indicate the experimental values.[33] The corresponding numerical data are given in Table 3. (b) Number of contact ion pairs in the aqueous solution at 6.1 mol kg^{-1} for NaCl and 4.8 mol kg^{-1} for KCl. The horizontal dotted line indicates the threshold value for supersaturation suggested by Benavides et al.[93]

The number of contact ion pairs (CIP) is defined as

$$n^{CIP} = 4\pi\rho_{\pm} \int_0^{r_{min}} g_{\pm}(r)r^2 dr', \quad (16)$$

where $\rho_{\pm}$ is the number density of cation or anion particles, $g_{\pm}(r)$ is the cation-anion radial distribution function, and r_{min} is the position of the first minimum of $g_{\pm}(r)$.[22, 49, 93] This property is closely related to the solubility of salt. In order to calculate n^{CIP}, we perform MD simulations of the aqueous solutions for 50 ns near the experimental solubility limit, 6.1 mol kg^{-1} for NaCl and 4.8 mol kg^{-1} for KCl. Figure 12b shows that n^{CIP} is large for models that underestimate the solubility. Formation of a large salt cluster is observed when n^{CIP} is very large (Figure S3). Benavides et al. proposed an empirical rule for classical MD simulations that the solution is supersaturated if n^{CIP} is larger than 0.5.[22, 93] This simple rule is satisfied for most of the models employed in this study, indicating that n^{CIP} is a useful property to roughly estimate the solubility without heavy computation as suggested by Benavides et al.

We compare the overall performance of the 20 ion models listed in Table 2 using the scheme of Vega and Abascal.[74] In this scheme, a score is given for each property and model. The score is defined as

$$M = \min\left\{ \text{anint}\left(10 - \left| \frac{100(X - X_{exp})}{P_{tol} X_{exp}} \right| \right), 0 \right\}, \quad (17)$$

where anint is the nearest integer function, X is the value of the property predicted by the model, X_{exp} is the corresponding experimental value, and P_{tol} is the tolerance given as a percentage. The score is 10 when the value predicted by the model is within 0.5 times the tolerance. The score is 0 when the deviation is larger than ten times of the tolerance. The tolerance is set to $P_{tol} = 1\%$ except for the ion-oxygen distance whose score is evaluated with $P_{tol} = 5\%$ reflecting the experimental uncertainty.[94] The score is not evaluated for the coordination number and the number of contact ion pairs because of the absence of accurate experimental data. We categorize the properties into five blocks: 1) thermodynamic properties of hydration at infinite dilution, i.e., G_{pair}, H_{pair}, and TS_{pair}, 2) self-diffusion coefficient of ion and ion-oxygen distance at infinite dilution, 3) viscosity, diffusion coefficient of water, and density at 3 mol kg^{-1}, 4) cation-anion distance, lattice energy, and enthalpy of solution of salt, and 5) solubility. The average over the scores of properties in each block is shown in Table 5 together with the global score, i.e., the average over all the blocks. The global score is also shown in Figure 13. Our three models are better than the other 17 models not only because of the quite good prediction for the solubility but also because of the relatively high score for the other blocks of properties. Among our ion parameter sets, the best one is that parameterized for SPC/E water because of the good score for the diffusion coefficient of ion at infinite dilution. It should be noted that the global score depends on the selection of properties. For example, if we focus only on the properties at infinite dilution, the best model becomes SPC/E-LSM. If the osmotic pressure of the aqueous solutions is considered, the score of TIP4P/2005-Madrid would be improved.[48]

Table 5. Scores of the five blocks of the properties and the average over them.

		G_{pair}, H_{pair}, and TS_{pair}	D^{ion} and IOD	3 mol kg⁻¹ ᵃ⁾	Salt ᵇ⁾	Solubility	Global score
SPC/E	This work	6.3	**8.2**	3.0	5.8	**8.0**	**6.3**
	JC	6.3	7.3	3.0	6.2	0.0	4.6
	LSM	**8.8**	7.8	3.2	4.5	0.0	4.9
	HMN1	6.7	5.5	0.0	3.7	0.0	3.2
	HMN2	7.0	7.2	**3.3**	5.3	0.0	4.6
	HMN3	6.5	6.8	**3.3**	**6.8**	0.0	4.7
	RH1	6.3	6.0	3.2	5.5	0.0	4.2
	RH2	6.3	4.7	1.5	5.5	4.0	4.4
	RH3	6.2	4.2	2.7	5.2	0.0	3.7
	Dang	6.5	5.2	2.8	4.2	0.0	3.7
	RDVH	6.7	**8.2**	2.7	4.0	3.5	5.0
	KBFF	5.7	7.0	3.2	5.7	0.0	4.3
TIP3P	This work	6.0	**4.8**	2.7	5.8	**9.0**	**5.7**
	JC	6.0	4.7	**3.0**	**6.0**	0.0	3.9
	LSM	**6.2**	4.5	**3.0**	4.8	0.0	3.7
	CHARMM	3.7	4.5	2.5	3.8	0.0	2.9
	AMBER	4.0	**4.8**	0.0	5.8	0.0	2.9
	OPLS	3.5	4.7	1.5	5.0	0.0	2.9
TIP4P /2005	This work	**6.3**	4.7	3.0	**5.8**	8.0	5.6
	Madrid	0.0	**5.8**	**3.3**	3.3	8.0	4.1

ᵃ⁾ Viscosity, diffusion coefficient of water, and density at 3 mol kg⁻¹.

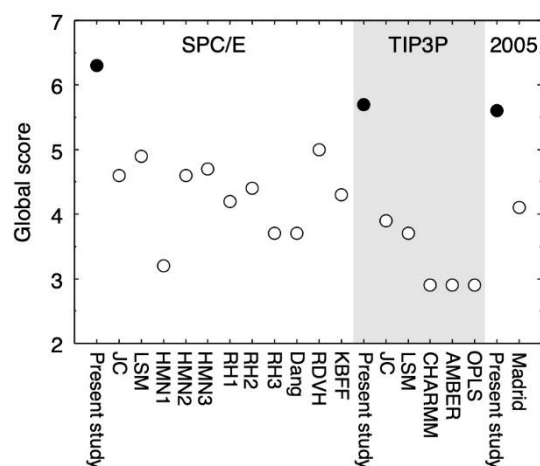ᵇ⁾ Cation-anion distance, lattice energy, and enthalpy of solution of salt.

Figure 13. Global score.

4. CONCLUSIONS

We have determined LJ parameters of Na^+, K^+, and Cl^- for the SPC/E, TIP3P, and TIP4P/2005 water models. The target properties are the hydration free energy, ion-oxygen distance in the solution phase, cation-anion distance in salt, and solubility. The relation between LJ energy parameter and the LJ size parameter that reproduces the experimental hydration free energy is approximated by a polynomial. The values of the LJ parameters are restricted to satisfy this polynomial in the parameterization. For each of the three water models, a set of ion LJ parameters is determined to reproduce the solubility using the potential energy of salt as a guide. The solubility is calculated from direct coexistence simulations in which a slab of salt is in contact with an aqueous solution.

The optimized LJ parameter sets are compared with 17 ion models using the scheme of Vega and Abascal.[74] The deviation from the experimental value is evaluated for 12 properties. The global score, which represents the overall performance of the ion model, is better for our models than for any of the 17 model.

All the simulations are performed at 298 K. The temperature dependence of the properties should be investigated in future work. There are some important properties other than those examined in this study. We have not calculated the activity of water in aqueous solutions which is related to colligative properties such as osmotic pressure and freezing-point depression.[48, 72] The activity coefficient of salt is also not calculated. The performance of our models with respect to those properties should also be investigated in future work.

The self-diffusion coefficient and hydration entropy of ion in water are determined mainly by the water-water interactions. MD simulation using the TIP3P water model cannot reproduce these properties because of the too weak water-water interactions. It is known that the performance of

the TIP3P model is also not good for pure water.[74] However, this water model has been frequently used in MD simulations of biomolecules because the CHARMM and AMBER force fields were designed to work with this water model. The solubility values predicted by the CHARMM and AMBER models are almost zero both for NaCl and KCl. In contrast, the LJ parameter set optimized for TIP3P in this study reproduces precisely the experimental solubility. This parameter set would be useful to examine properties of biomolecules in dense aqueous NaCl or KCl solutions without artifacts arising from ion aggregation.[95-98]

The SPC/E model reproduces well various thermodynamic and dynamic properties of pure water due to the so called self-polarization term that results in water-water interactions stronger than those of water models without this correction.[74] The ion parameter set optimized for the SPC/E model in this study, which exhibits the highest global score, is recommended for MD simulations of aqueous NaCl and KCl solutions without biomolecules. In particular, the model would be useful to study kinetics of precipitation of salt in water.[99-103] A drawback is that the melting temperature of ice Ih described by SPC/E, 215 K, is much lower than the experimental value. The coexistence of ice and dense aqueous electrolyte solutions can be seen not only in laboratory but also in nature.[104-108] Our parameter set for the TIP4P/2005 model might be useful for MD simulations of such systems because TIP4P/2005 reproduces the melting temperature and ice properties fairly well.[47, 53]

ACKNOWLEDGMENTS

efficiency energy creation, conversion/storage and use). MD simulations were performed on the computers at Research Center for Computational Science, Okazaki, Japan.

SUPPORTING INFORMATION

The supporting information is available free of charge via the Internet at http://pubs.acs.org

Effects of changes in σ and ε on the LJ potential (Figure S1), enthalpy of solution at 0.5, 1, and 3 mol kg^{-1} (Figure S2), snapshots of MD simulations of the aqueous NaCl solution near the experimental solubility limit (Figure S3), LJ parameters of the employed ion models (Table S1), properties of Na^{+} calculated from five independent simulations (Table S2), coefficients in Eq .14 (Table S3), thermodynamic properties of ion hydration (Table S4), thermodynamic properties of ion pairs (Table S5), Henry's law standard state chemical potential of salt (Table S6), self-diffusion coefficients of ions (Table S7), structural properties in the solution at infinite dilution (Table S8), properties of the solutions at 3 mol kg^{-1} (Table S9), salt properties (Table S10), and solubility values (Table S11).

REFERENCES

1. Marcus, Y. Ionic Radii in Aqueous Solutions. *Chem. Rev.* **1988**, *88*, 1475-1498.

2. Marcus, Y. Effect of Ions on the Structure of Water: Structure Making and Breaking. *Chem. Rev.* **2009**, *109*, 1346-1370.

3. Ohtaki, H.; Radnai, T. Structure and Dynamics of Hydrated Ions. *Chem. Rev.* **1993**, *93*, 1157-1204.

4. Flanagin, L. W.; Balbuena, P. B.; Johnston, K. P.; Rossky, P. J. Temperature and Density Effects on an S_N2 Reaction in Supercritical Water. *J. Phys. Chem.* **1995**, *99*, 5196-5205.

5. Balbuena, P. B.; Johnston, K. P.; Rossky, P. J. Molecular Dynamics Simulation of Electrolyte Solutions in Ambient and Supercritical Water. 1. Ion Solvation. *J. Phys. Chem.* **1996**, *100*, 2706-2715.

6. Lynden-Bell, R. M.; Rasaiah, J. C. From Hydrophobic to Hydrophilic Behaviour: A Simulation Study of Solvation Entropy and Free Energy of Simple Solutes. *J. Chem. Phys.* **1997**, *107*, 1981-1991.

7. Parsons, D. F.; Bostrom, M.; Lo Nostro, P.; Ninham, B. W. Hofmeister Effects: Interplay of Hydration, Nonelectrostatic Potentials, and Ion Size. *Phys. Chem. Chem. Phys.* **2011**, *13*, 12352-12367.

8. Thomas, A. S.; Elcock, A. H. Molecular Dynamics Simulations of Hydrophobic Associations in Aqueous Salt Solutions Indicate a Connection between Water Hydrogen Bonding and the Hofmeister Effect. *J. Am. Chem. Soc.* **2007**, *129*, 14887-14898.

9. Nihonyanagi, S.; Yamaguchi, S.; Tahara, T. Counterion Effect on Interfacial Water at Charged Interfaces and Its Relevance to the Hofmeister Series. *J. Am. Chem. Soc.* **2014**, *136*, 6155-6158.

10.   Bagchi, B.; Jana, B. Solvation Dynamics in Dipolar Liquids. *Chem. Soc. Rev.* **2010**, *39*, 1936-1954.

11.   Yagasaki, T.; Iwahashi, K.; Saito, S.; Ohmine, I. A Theoretical Study on Anomalous Temperature Dependence of pK_w of Water. *J. Chem. Phys.* **2005**, *122*, 144504.

12.   Roux, B.; Schulten, K. Computational Studies of Membrane Channels. *Structure* **2004**, *12*, 1343-1351.

13.   Jungwirth, P.; Tobias, D. J. Specific Ion Effects at the Air/Water Interface. *Chem. Rev.* **2006**, *106*, 1259-1281.

14.   Klotz, S.; Bove, L. E.; Strassle, T.; Hansen, T. C.; Saitta, A. M. The Preparation and Structure of Salty Ice VII under Pressure. *Nat. Mater.* **2009**, *8*, 405-409.

15.   Hess, B.; Kutzner, C.; van der Spoel, D.; Lindahl, E. Gromacs 4: Algorithms for Highly Efficient, Load-Balanced, and Scalable Molecular Simulation. *J. Chem. Theory Comput.* **2008**, *4*, 435-447.

16.   Van der Spoel, D.; Lindahl, E.; Hess, B.; Groenhof, G.; Mark, A. E.; Berendsen, H. J. C. Gromacs: Fast, Flexible, and Free. *J. Comput. Chem.* **2005**, *26*, 1701-1718.

17.   Case, D. A.; Cheatham, T. E., 3rd; Darden, T.; Gohlke, H.; Luo, R.; Merz, K. M., Jr.; Onufriev, A.; Simmerling, C.; Wang, B.; Woods, R. J. The Amber Biomolecular Simulation Programs. *J. Comput. Chem.* **2005**, *26*, 1668-1688.

18.   Salomon-Ferrer, R.; Case, D. A.; Walker, R. C. An Overview of the Amber Biomolecular Simulation Package. *Wiley Interdiscip. Rev.: Comput. Mol. Sci.* **2013**, *3*, 198-210.

19.   Plimpton, S. Fast Parallel Algorithms for Short-Range Molecular Dynamics. *J. Comput. Phys.* **1995**, *117*, 1-19.

20.   Andoh, Y.; Yoshii, N.; Fujimoto, K.; Mizutani, K.; Kojima, H.; Yamada, A.; Okazaki, S.;
        Kawaguchi, K.; Nagao, H.; Iwahashi, K.; Mizutani, F.; Minami, K.; Ichikawa, S.;
        Komatsu, H.; Ishizuki, S.; Takeda, Y.; Fukushima, M. Modylas: A Highly Parallelized
        General-Purpose Molecular Dynamics Simulation Program for Large-Scale Systems with
        Long-Range Forces Calculated by Fast Multipole Method (FMM) and Highly Scalable
        Fine-Grained New Parallel Processing Algorithms. *J. Chem. Theory Comput.* **2013**, *9*,
        3201-3209.

21.   Mester, Z.; Panagiotopoulos, A. Z. Temperature-Dependent Solubilities and Mean Ionic
        Activity Coefficients of Alkali Halides in Water from Molecular Dynamics Simulations.
        J. Chem. Phys. **2015**, *143*, 044505.

22.   Benavides, A. L.; Aragones, J. L.; Vega, C. Consensus on the Solubility of NaCl in
        Water from Computer Simulations Using the Chemical Potential Route. *J. Chem. Phys.*
        2016, *144*, 124504.

23.   Ladd, A. J. C.; Woodcock, L. V. Triple-Point Coexistence Properties of the Lennard-
        Jones System. *Chem. Phys. Lett.* **1977**, *51*, 155-159.

24.   Joung, I. S.; Cheatham, T. E. Molecular Dynamics Simulations of the Dynamic and
        Energetic Properties of Alkali and Halide Ions Using Water-Model-Specific Ion
        Parameters. *J. Phys. Chem. B* **2009**, *113*, 13279-13290.

25.   Manzanilla-Granados, H. M.; Saint-Martin, H.; Fuentes-Azcatl, R.; Alejandre, J. Direct
        Coexistence Methods to Determine the Solubility of Salts in Water from Numerical
        Simulations. Test Case NaCl. *J. Phys. Chem. B* **2015**, *119*, 8389-8396.

26.   Kobayashi, K.; Liang, Y.; Sakka, T.; Matsuoka, T. Molecular Dynamics Study of Salt-Solution Interface: Solubility and Surface Charge of Salt in Water. *J. Chem. Phys.* **2014**, *140*, 144705.

27.   Espinosa, J. R.; Young, J. M.; Jiang, H.; Gupta, D.; Vega, C.; Sanz, E.; Debenedetti, P. G.; Panagiotopoulos, A. Z. On the Calculation of Solubilities via Direct Coexistence Simulations: Investigation of NaCl Aqueous Solutions and Lennard-Jones Binary Mixtures. *J. Chem. Phys.* **2016**, *145*, 154111.

28.   Auffinger, P.; Cheatham, T. E.; Vaiana, A. C. Spontaneous Formation of KCl Aggregates in Biomolecular Simulations: A Force Field Issue? *J. Chem. Theory Comput.* **2007**, *3*, 1851-1859.

29.   Savelyev, A.; Papoian, G. A. Electrostatic, Steric, and Hydration Interactions Favor Na^+ Condensation around DNA Compared with K^+. *J. Am. Chem. Soc.* **2006**, *128*, 14506-14518.

30.   Savelyev, A.; Papoian, G. A. Inter-DNA Electrostatics from Explicit Solvent Molecular Dynamics Simulations. *J. Am. Chem. Soc.* **2007**, *129*, 6060-6061.

31.   Vaiana, A. C.; Westhof, E.; Auffinger, P. A Molecular Dynamics Simulation Study of an Aminoglycoside/A-Site RNA Complex: Conformational and Hydration Patterns. *Biochimie* **2006**, *88*, 1061-1073.

32.   Chen, A. A.; Pappu, R. V. Parameters of Monovalent Ions in the Amber-99 Forcefield: Assessment of Inaccuracies and Proposed Improvements. *J. Phys. Chem. B* **2007**, *111*, 11884-11887.

33.   *CRC Handbook of Chemistry and Physics*, 89 ed.; CRC Press: Boca Raton, 2008.

34.   Berendsen, H. J. C.; Grigera, J. R.; Straatsma, T. P. The Missing Term in Effective Pair Potentials. *J. Phys. Chem.* **1987**, *91*, 6269-6271.

35.   Joung, I. S.; Cheatham, T. E. Determination of Alkali and Halide Monovalent Ion Parameters for Use in Explicitly Solvated Biomolecular Simulations. *J. Phys. Chem. B* **2008**, *112*, 9020-9041.

36.   Moučka, F.; Nezbeda, I.; Smith, W. R. Molecular Force Fields for Aqueous Electrolytes: SPC/E-Compatible Charged LJ Sphere Models and Their Limitations. *J. Chem. Phys.* **2013**, *138*, 154102.

37.   Kolafa, J. Solubility of Nacl in Water and Its Melting Point by Molecular Dynamics in the Slab Geometry and a New BK3-Compatible Force Field. *J. Chem. Phys.* **2016**, *145*, 204509.

38.   Horinek, D.; Mamatkulov, S. I.; Netz, R. R. Rational Design of Ion Force Fields Based on Thermodynamic Solvation Properties. *J. Chem. Phys.* **2009**, *130*, 124507.

39.   Reif, M. M.; Hünenberger, P. H. Computation of Methodology-Independent Single-Ion Solvation Properties from Molecular Simulations. IV. Optimized Lennard-Jones Interaction Parameter Sets for the Alkali and Halide Ions in Water. *J. Chem. Phys.* **2011**, *134*, 144104.

40.   Dang, L. X. Mechanism and Thermodynamics of Ion Selectivity in Aqueous Solutions of 18-Crown-6 Ether: A Molecular Dynamics Study. *J. Am. Chem. Soc.* **1995**, *117*, 6954-6960.

41.   Reiser, S.; Deublein, S.; Vrabec, J.; Hasse, H. Molecular Dispersion Energy Parameters for Alkali and Halide Ions in Aqueous Solution. *J. Chem. Phys.* **2014**, *140*, 044504.

42.	Gee, M. B.; Cox, N. R.; Jiao, Y.; Bentenitis, N.; Weerasinghe, S.; Smith, P. E. A Kirkwood-Buff Derived Force Field for Aqueous Alkali Halides. *J. Chem. Theory Comput.* **2011**, *7*, 1369-1380.

43.	Smith, D. E.; Dang, L. X. Computer-Simulations of NaCl Association in Polarizable Water. *J. Chem. Phys.* **1994**, *100*, 3757-3766.

44.	Roux, B. Valence Selectivity of the Gramicidin Channel: A Molecular Dynamics Free Energy Perturbation Study. *Biophys. J.* **1996**, *71*, 3177-3185.

45.	Deublein, S.; Vrabec, J.; Hasse, H. A Set of Molecular Models for Alkali and Halide Ions in Aqueous Solution. *J. Chem. Phys.* **2012**, *136*, 084501.

46.	Jorgensen, W. L.; Chandrasekhar, J.; Madura, J. D.; Impey, R. W.; Klein, M. L. Comparison of Simple Potential Functions for Simulating Liquid Water. *J. Chem. Phys.* **1983**, *79*, 926-935.

47.	Abascal, J. L. F.; Vega, C. A General Purpose Model for the Condensed Phases of Water: TIP4P/2005. *J. Chem. Phys.* **2005**, *123*, 234505.

48.	Benavides, A. L.; Portillo, M. A.; Chamorro, V. C.; Espinosa, J. R.; Abascal, J. L. F.; Vega, C. A Potential Model for Sodium Chloride Solutions Based on the TIP4P/2005 Water Model. *J. Chem. Phys.* **2017**, *147*, 104501.

49.	Zeron, I. M.; Abascal, J. L. F.; Vega, C. A Force Field of Li^+, Na^+, K^+, Mg^{2+}, Ca^{2+}, Cl^-, and SO_4^{2-} in Aqueous Solution Based on the TIP4P/2005 Water Model and Scaled Charges for the Ions. *J. Chem. Phys.* **2019**, *151*, 134504.

50.	Li, P.; Song, L. F.; Merz, K. M. Systematic Parameterization of Monovalent Ions Employing the Nonbonded Model. *J. Chem. Theory Comput.* **2015**, *11*, 1645-1657.

51. Starr, F. W.; Harrington, S.; Sciortino, F.; Stanley, H. E. Slow Dynamics of Water under Pressure. *Phys. Rev. Lett.* **1999**, *82*, 3629-3632.

52. Yagasaki, T.; Saito, S. Ultrafast Intermolecular Dynamics of Liquid Water: A Theoretical Study on Two-Dimensional Infrared Spectroscopy. *J. Chem. Phys.* **2008**, *128*, 154521.

53. Conde, M. M.; Gonzalez, M. A.; Abascal, J. L.; Vega, C. Determining the Phase Diagram of Water from Direct Coexistence Simulations: The Phase Diagram of the TIP4P/2005 Model Revisited. *J. Chem. Phys.* **2013**, *139*, 154505.

54. Aragones, J. L.; Vega, C. Plastic Crystal Phases of Simple Water Models. *J. Chem. Phys.* **2009**, *130*, 244504.

55. Yagasaki, T.; Matsumoto, M.; Tanaka, H. Phase Diagrams of TIP4P/2005, SPC/E, and TIP5P Water at High Pressure. *J. Phys. Chem. B* **2018**, *122*, 7718-7725.

56. Chandrasekhar, J.; Spellmeyer, D. C.; Jorgensen, W. L. Energy Component Analysis for Dilute Aqueous Solutions of Lithium(1+), Sodium(1+), Fluoride(1-), and Chloride(1-) Ions. *J. Am. Chem. Soc.* **1984**, *106*, 903-910.

57. Nosé, S. A Molecular Dynamics Method for Simulations in the Canonical Ensemble. *Mol. Phys.* **1984**, *52*, 255-268.

58. Hoover, W. G. Canonical Dynamics: Equilibrium Phase-Space Distributions. *Phys. Rev. A* **1985**, *31*, 1695-1697.

59. Nosé, S.; Klein, M. L. Constant Pressure Molecular Dynamics for Molecular Systems. *Mol. Phys.* **1983**, *50*, 1055-1076.

60. Allen, M. P.; Tildesley, D. J., Computer Simulation of Liquids. Clarendon press: Oxford, 1987.

61.   Darden, T.; York, D.; Pedersen, L. Particle Mesh Ewald: An N·Log(N) Method for Ewald Sums in Large Systems. *J. Chem. Phys.* **1993**, *98*, 10089-10092.

62.   Essmann, U.; Perera, L.; Berkowitz, M. L.; Darden, T.; Lee, H.; Pedersen, L. G. A Smooth Particle Mesh Ewald Method. *J. Chem. Phys.* **1995**, *103*, 8577-8593.

63.   Radenović, N.; van Enckevort, W.; Verwer, P.; Vlieg, E. Growth and Characteristics of the {1 1 1} Nacl Crystal Surface Grown from Solution. *Surf Sci.* **2003**, *523*, 307-315.

64.   Beutler, T. C.; Mark, A. E.; van Schaik, R. C.; Gerber, P. R.; van Gunsteren, W. F. Avoiding Singularities and Numerical Instabilities in Free Energy Calculations Based on Molecular Simulations. *Chem. Phys. Lett.* **1994**, *222*, 529-539.

65.   Bennett, C. H. Efficient Estimation of Free Energy Differences from Monte Carlo Data. *J. Comput. Phys.* **1976**, *22*, 245-268.

66.   Yeh, I.-C.; Hummer, G. System-Size Dependence of Diffusion Coefficients and Viscosities from Molecular Dynamics Simulations with Periodic Boundary Conditions. *J. Phys. Chem. B* **2004**, *108*, 15873-15879.

67.   González, M. A.; Abascal, J. L. F. The Shear Viscosity of Rigid Water Models. *J. Chem. Phys.* **2010**, *132*, 096101.

68.   Robinson, R. A.; Stokes, R. H., *Electrolyte Solutions*; Butterworths: London, 1959.

69.   Benson, G. C.; Gordon, A. R. A Reinvestigation of the Conductance of Aqueous Solutions of Potassium Chloride, Sodium Chloride, and Potassium Bromide at Temperatures from 15° to 45°C. *J. Chem. Phys.* **1945**, *13*, 473-474.

70.   Schmid, R.; Miah, A. M.; Sapunov, V. N. A New Table of the Thermodynamic Quantities of Ionic Hydration: Values and Some Applications (Enthalpy-Entropy Compensation and Born Radii). *Phys. Chem. Chem. Phys.* **2000**, *2*, 97-102.

71.   Marcus, Y. Thermodynamics of Solvation of Ions. Part 5. Gibbs Free Energy of Hydration at 298.15 K. *J. Chem. Soc., Faraday Trans.* **1991**, *87*, 2995-2999.

72.   Mester, Z.; Panagiotopoulos, A. Z. Mean Ionic Activity Coefficients in Aqueous NaCl Solutions from Molecular Dynamics Simulations. *J. Chem. Phys.* **2015**, *142*, 044507.

73.   Wagman, D. D.; Evans, W. H.; Parker, V. B.; Schumm, R. H.; Halow, I.; Bailey, S. M.; Churney, K. L.; Nuttall, R. L. The NBS Tables of Chemical Thermodynamic Properties. Selected Values for Inorganic and C1 and C2 Organic Substances in SI Units. *J. Phys. Chem. Ref. Data* **1982**, *11*, Suppl. 2.

74.   Vega, C.; Abascal, J. L. Simulating Water with Rigid Non-Polarizable Models: A General Perspective. *Phys. Chem. Chem. Phys.* **2011**, *13*, 19663-19688.

75.   Frank, H. S.; Wen, W.-Y. Ion-Solvent Interaction. Structural Aspects of Ion-Solvent Interaction in Aqueous Solutions: A Suggested Picture of Water Structure. *Discuss. Faraday Soc.* **1957**, *24*, 133-140.

76.   Koneshan, S.; Rasaiah, J. C.; Lynden-Bell, R. M.; Lee, S. H. Solvent Structure, Dynamics, and Ion Mobility in Aqueous Solutions at 25 °C. *J. Phys. Chem. B* **1998**, *102*, 4193-4204.

77.   Bankura, A.; Carnevale, V.; Klein, M. L. Hydration Structure of Salt Solutions from ab Initio Molecular Dynamics. *J. Chem. Phys.* **2013**, *138*, 014501.

78.   Rowley, C. N.; Roux, B. t. The Solvation Structure of Na^+ and K^+ in Liquid Water Determined from High Level ab Initio Molecular Dynamics Simulations. *J. Chem. Theory Comput.* **2012**, *8*, 3526-3535.

79.   Shiga, M.; Masia, M. Boundary Based on Exchange Symmetry Theory for Multilevel Simulations. II. Multiple Time Scale Approach. *J. Chem. Phys.* **2013**, *139*, 144103.

80. Tongraar, A.; J, T. T.; Rujirawat, S.; Limpijumnong, S. Structure of the Hydrated Ca^{2+} and Cl^{-}: Combined X-Ray Absorption Measurements and QM/MM MD Simulations Study. *Phys. Chem. Chem. Phys.* **2010**, *12*, 10876-10887.

81. Mahler, J.; Persson, I. A Study of the Hydration of the Alkali Metal Ions in Aqueous Solution. *Inorg. Chem.* **2012**, *51*, 425-438.

82. Noskov, S. Y.; Berneche, S.; Roux, B. Control of Ion Selectivity in Potassium Channels by Electrostatic and Dynamic Properties of Carbonyl Ligands. *Nature* **2004**, *431*, 830-834.

83. Bostick, D. L.; Brooks, C. L. Selective Complexation of K^{+} and Na^{+} in Simple Polarizable Ion-Ligating Systems. *J. Am. Chem. Soc.* **2010**, *132*, 13185-13187.

84. Varma, S.; Rempe, S. B. Structural Transitions in Ion Coordination Driven by Changes in Competition for Ligand Binding. *J. Am. Chem. Soc.* **2008**, *130*, 15405-15419.

85. Kim, J. S.; Wu, Z.; Morrow, A. R.; Yethiraj, A.; Yethiraj, A. Self-Diffusion and Viscosity in Electrolyte Solutions. *J. Phys. Chem. B* **2012**, *116*, 12007-12013.

86. Yao, Y.; Berkowitz, M. L.; Kanai, Y. Communication: Modeling of Concentration Dependent Water Diffusivity in Ionic Solutions: Role of Intermolecular Charge Transfer. *J. Chem. Phys.* **2015**, *143*, 241101.

87. Leontyev, I. V.; Stuchebrukhov, A. A. Electronic Continuum Model for Molecular Dynamics Simulations. *J. Chem. Phys.* **2009**, *130*, 085102.

88. Kann, Z. R.; Skinner, J. L. A Scaled-Ionic-Charge Simulation Model That Reproduces Enhanced and Suppressed Water Diffusion in Aqueous Salt Solutions. *J. Chem. Phys.* **2014**, *141*, 104507.

89. Müller, K. J.; Hertz, H. G. A Parameter as an Indicator for Water−Water Association in Solutions of Strong Electrolytes. *J. Phys. Chem.* **1996**, *100*, 1256-1265.

90. Laliberté, M.; Cooper, W. E. Model for Calculating the Density of Aqueous Electrolyte Solutions. *J. Chem. Eng. Data* **2004**, *49*, 1141-1151.

91. Laliberté, M. Model for Calculating the Viscosity of Aqueous Solutions. *J. Chem. Eng. Data* **2007**, *52*, 1507-1508.

92. Sanahuja, A.; Cesari, E. Enthalpy of Solution of KCl and NaCl in Water at 298.15 K. *J. Chem. Thermodyn.* **1984**, *16*, 1195-1202.

93. Benavides, A. L.; Portillo, M. A.; Abascal, J. L. F.; Vega, C. Estimating the Solubility of 1:1 Electrolyte Aqueous Solutions: The Chemical Potential Difference Rule. *Mol. Phys.* **2017**, *115*, 1301-1308.

94. Mancinelli, R.; Botti, A.; Bruni, F.; Ricci, M. A.; Soper, A. K. Hydration of Sodium, Potassium, and Chloride Ions in Solution and the Concept of Structure Maker/Breaker. *J. Phys. Chem. B* **2007**, *111*, 13570-13577.

95. Oncins, G.; Garcia-Manyes, S.; Sanz, F. Study of Frictional Properties of a Phospholipid Bilayer in a Liquid Environment with Lateral Force Microscopy as a Function of NaCl Concentration. *Langmuir* **2005**, *21*, 7373-7379.

96. Vácha, R.; Siu, S. W. I.; Petrov, M.; Böckmann, R. A.; Barucha-Kraszewska, J.; Jurkiewicz, P.; Hof, M.; Berkowitz, M. L.; Jungwirth, P. Effects of Alkali Cations and Halide Anions on the Dopc Lipid Membrane. *J. Phys. Chem. A* **2009**, *113*, 7235-7243.

97. Lipfert, J.; Doniach, S.; Das, R.; Herschlag, D. Understanding Nucleic Acid-Ion Interactions. *Annu. Rev. Biochem* **2014**, *83*, 813-841.

98.   Šponer, J.; Bussi, G.; Krepl, M.; Banáš, P.; Bottaro, S.; Cunha, R. A.; Gil-Ley, A.;
Pinamonti, G.; Poblete, S.; Jurečka, P.; Walter, N. G.; Otyepka, M. RNA Structural
Dynamics as Captured by Molecular Simulations: A Comprehensive Overview. *Chem.
Rev.* **2018**, *118*, 4177-4338.

99.   Zahn, D. Atomistic Mechanism of NaCl Nucleation from an Aqueous Solution. *Phys.
Rev. Lett.* **2004**, *92*, 040801.

100.   Chakraborty, D.; Patey, G. N. How Crystals Nucleate and Grow in Aqueous NaCl
Solution. *J. Phys. Chem. Lett.* **2013**, *4*, 573-578.

101.   Zimmermann, N. E. R.; Vorselaars, B.; Quigley, D.; Peters, B. Nucleation of NaCl from
Aqueous Solution: Critical Sizes, Ion-Attachment Kinetics, and Rates. *J. Am. Chem. Soc.*
2015, *137*, 13352-13361.

102.   Jiang, H.; Haji-Akbari, A.; Debenedetti, P. G.; Panagiotopoulos, A. Z. Forward Flux
Sampling Calculation of Homogeneous Nucleation Rates from Aqueous NaCl Solutions.
J. Chem. Phys. **2018**, *148*, 044505.

103.   Jiang, H.; Debenedetti, P. G.; Panagiotopoulos, A. Z. Communication: Nucleation Rates
of Supersaturated Aqueous Nacl Using a Polarizable Force Field. *J. Chem. Phys.* **2018**,
149, 141102.

104.   Petrenko, V. F.; Whitworth, R. W., *Physics of Ice*; Oxford University Press: Oxford,
1999.

105.   Takenaka, N.; Ueda, A.; Daimon, T.; Bandow, H.; Dohmaru, T.; Maeda, Y. Acceleration
Mechanism of Chemical Reaction by Freezing: The Reaction of Nitrous Acid with
Dissolved Oxygen. *J. Phys. Chem.* **1996**, *100*, 13874-13884.

106.   Watanabe, H.; Otsuka, T.; Harada, M.; Okada, T. Imbalance between Anion and Cation Distribution at Ice Interface with Liquid Phase in Frozen Electrolyte as Evaluated by Fluorometric Measurements of pH. *J. Phys. Chem. C* **2014**, *118*, 15723-15731.

107.   Tasaki, Y.; Okada, T. Up to 4 Orders of Magnitude Enhancement of Crown Ether Complexation in an Aqueous Phase Coexistent with Ice. *J. Am. Chem. Soc.* **2012**, *134*, 6128-6131.

108.   Obbard, R. W.; Troderman, G.; Baker, I. Imaging Brine and Air Inclusions in Sea Ice Using Micro-X-Ray Computed Tomography. *Journal of Glaciology* **2017**, *55*, 1113-1115.